Nanoscale

PAPER

View Article Online
View Journal | View Issue

Cite this: *Nanoscale*, 2022, **14**, 15141

Substrate stiffness reduces particle uptake by epithelial cells and macrophages in a size-dependent manner through mechanoregulation†

Aaron Lee, [a] Mauro Sousa de Almeida, [a] Daela Milinkovic,[a] Dedy Septiadi, [a] Patricia Taladriz-Blanco, [a,b] Céline Loussert-Fonta, [a] Sandor Balog, [a] Amelie Bazzoni,[a] Barbara Rothen-Rutishauser [a] and Alke Petri-Fink *[a,c]

Cells continuously exert forces on their environment and respond to changes in mechanical forces by altering their behaviour. Many pathologies such as cancer and fibrosis are hallmarked by dysregulation in the extracellular matrix, driving aberrant behaviour through mechanotransduction pathways. We demonstrate that substrate stiffness can be used to regulate cellular endocytosis of particles in a size-dependent fashion. Culture of A549 epithelial cells and J774A.1 macrophages on polystyrene/glass (stiff) and polydimethylsiloxane (soft) substrates indicated that particle uptake is increased up to six times for A549 and two times for macrophages when cells are grown in softer environments. Furthermore, we altered surface characteristics through the attachment of submicron-sized particles as a method to locally engineer substrate stiffness and topography to investigate the biomechanical changes which occurred within adherent epithelial cells, *i.e.* characterization of A549 cell spreading and focal adhesion maturation. Consequently, decreasing substrate rigidity and particle-based topography led to a reduction of focal adhesion size. Moreover, expression levels of Yes-associated protein were found to correlate with the degree of particle endocytosis. A thorough appreciation of the mechanical cues may lead to improved solutions to optimize nanomedicine approaches for treatment of cancer and other diseases with abnormal mechanosignalling.

Received 11th July 2022,
Accepted 30th September 2022

DOI: 10.1039/d2nr03792k

rsc.li/nanoscale

Introduction

Physical cues within the cellular microenvironment play a vital role in defining cellular behaviour through the regulation of processes such as proliferation and differentiation through mechanotransduction.[1] The interplay between the physical niche and cell behaviour is a prominent feature in development as well as in ageing, inflammation and cancer.[2–4] Mimicking mechanobiological cues can recapitulate features present during tissue development as well as improving host integration of medical devices.[5,6] Designing new material interfaces and systems to synergise and exploit mechanical cues is emerging as a powerful approach to modulate biological responses.

To date, a considerable effort has been spent trying to characterize the physicochemical properties of engineered nanomaterials in order to understand their interaction with cells, tissues and organisms.[7] Features such as particle size, shape, surface chemistry are commonly cited as key properties that govern particle behaviour, cellular interactions and endocytosis. Despite this, predicting cellular endocytosis remains an ongoing challenge, hindering effective use of nanoparticles for medical applications. Increasingly, the mechanical response of nanoparticles is being shown to be a relevant parameter in influencing internalization.[8,9] Particle rigidity has been shown theoretically and empirically to impact the ability of a particle to enter a cell, with stiffer particles often being favoured.[10–12]

Part of the reason for the discrepancy between *in vitro* and *in vivo* exposure is because the interaction between nanoparticles and cells is not wholly dependent on particle physicochemical properties. Huang *et al.* demonstrated that by culturing cells on substrates with different stiffness, they could exhibit different degrees of particle uptake, with stiffer substrates promoting spreading and internalisation.[13] As cells can respond differently to stiffness cues, characterising their impact on uptake is critical for improving nanoparticle-based therapy approaches. Moreover, cancer cells exhibit different

[a]*Adolphe Merkle Institute, University of Fribourg, Chemin des Verdiers 4, 1700 Fribourg, Switzerland. E-mail: alke.fink@unifr.ch*
[b]*International Iberian Nanotechnology Laboratory (INL), Water Quality Group, Av. Mestre José Veiga s/n, 4715-330 Braga, Portugal*
[c]*Department of Chemistry, University of Fribourg, Chemin du Musée 9, 1700 Fribourg, Switzerland*

† Electronic supplementary information (ESI) available. See DOI: https://doi.org/10.1039/d2nr03792k

mechanical properties associated with their metastatic potential and are a major clinical target.[14,15]

(Nano)particles offer a unique approach to designing novel biomaterial interfaces as they themselves generate physical cues that can impact cell behaviour.[16,17] These surfaces possess their own local stiffness and topographical cues that can alter cellular mechanotransduction.[12,18] It is worth noting that suspended particles can adsorb non-specifically to surfaces and cell membranes, generating additional interactions.[19] As particles attach to various surfaces, they can create texture and roughness that influences cell adhesion and behaviour. Furthermore, the topographical cues generated by the particles themselves can promote local endocytosis at the surface interface.[20–22] Understanding how substrate characteristics, particle–surface and particle–cell interactions can alter cell behaviour is critical to predicting and directing uptake.

Building upon the idea that the mechanical properties of the cell substrate influence phenotype and that the properties of particles influences particle endocytosis, we asked how mechanical cues from the cell environment consequently influence endocytosis of particles in suspension and whether any size-dependent effects would be present. In order to pursue this reasoning, we compared particle uptake for cells cultured on stiff standard tissue culture polystyrene (TCPS) to more compliant substrates based on polydimethylsiloxane (PDMS). Entry of particles into a cell is dependent on size and receptor interactions, with larger particles are mainly internalised by either phagocytosis or macropinocytosis.[7] Non-phagocytic alveolar lung epithelial cells (A549) and phagocytic murine macrophages (J774A.1) cells were exposed to 120 nm and 360 nm silica particles to assess how mechanical cues affected uptake. Moreover, particles can also attach to surfaces and alter cell adhesion and uptake by changing the physical environment of the cell.[12,18] Mechanoregulation of particle uptake arising from stiffness and topographical cues was evaluated by assembling hard silica particles on top of softer PDMS surfaces. Examination of the mechanoregulatory network from focal adhesion and cell spreading characteristics to Yes-associated protein (YAP) expression has allowed a clearer map of how physical cues from the cell microenvironment can modulate internalization of particles. We show that increasing mechanical complexity by simultaneously providing different types of physical cues such as substrate stiffness and particle-based topography can be used to derive insight into particle–cell interactions. This understanding of how the physical cues shape cell behaviour can be used to design better predictive models for characterization of particle–cell interactions.

Results and discussion

Herein, the role of substrate stiffness on size-dependent particle endocytosis was determined by exposing two distinct cell types (A549 and J774A.1) to 120 nm and 360 nm silica particles. Mechanical cues can modulate various cell behaviours, including the interactions between particles and cells as well as subsequent internalization. As physiological cell environments differ significantly from standard *in vitro* culture conditions, it is imperative to more closely mimic the biophysical properties of tissues *in situ* in order to obtain a more accurate understanding. Cells were cultured on rigid standard cell culture materials such as TCPS and glass, which possess Young's moduli in the gigapascal range, and on softer PDMS, which can be tuned to exhibit a range of stiffness values from several kilopascals to a few megapascals. We have observed that particles in suspension can attach to biomaterial surfaces to form a layer and consequently give rise to localised interactions such as alterations to adhesion and particle clearance.[12,18] To be able to differentiate between particles in suspension and substrate adsorbed particles following internalization, two different fluorophores were used to label synthesised silica. For particles added in suspension, Cyanine5 (Cy5) was selected, while for particles used to decorate the PDMS, BODIPY (BDP) was chosen as both fluorophores had been shown to be suitable for cell experiments.[23]

Mechanical regulation of particle endocytosis was examined on stiff (TCPS), intermediate (PDMS 10 : 1) and soft (PDMS 40 : 1) substrates. In order to understand whether mechanoregulation affected all particles equally or showed size-dependent effects, two particle sizes were chosen (Fig. 1a). Particle characteristics such as morphology, size and size distribution for silica particles were characterised by transmission electron microscopy (TEM): Cy5-small (d_{TEM} = 120 nm), Cy5-large (d_{TEM} = 360 nm) and BDP (d_{TEM} = 420 nm) (Fig. 1b and c, and S1a and b, ESI†). Hydrodynamic diameter was assessed through dynamic light scattering (DLS) in ultrapure water as a dilute suspension. Measurements performed in ultrapure water yielded hydrodynamic diameters for Cy5-small (d_{DLS} = 145 nm), Cy5-large (d_{DLS} = 360 nm) and BDP (d_{DLS} = 420 nm). Resultant sizes were congruent with sizes obtained from imaging. Zeta potential analysis was conducted in ultrapure water with dilute suspensions with all particles exhibiting strongly negative zeta potential values, reflecting the presence of surface silanol groups (Table S1, ESI†).[24]

Colloidal stability of silica particles added to cells was assessed in serum supplemented cell culture medium at 37 °C by DLS. Hydrodynamic size was determined at 0 h and 6 h for Cy5-small and Cy5-large silica particles with no substantial changes in apparent size noted as would be expected for aggregation processes (Fig. 1b and c and Fig. S2†). Silica particles remain dispersed in complex cell culture medium due to the formation of the protein corona which helps maintain colloidal stability.[25,26]

To examine the impact of substrate stiffness on cellular endocytosis, cells were grown in a standard 6-well cell culture plate and compared to cells grown on PDMS 10 : 1 and PDMS 40 : 1. PDMS is a commonly utilised material for altering cell behaviour as a function of stiffness and offers excellent optical properties, stability and stretchability for dynamic culture systems.[27–30] The Young's modulus of formulated PDMS was determined by creating tensile samples followed by elongation under uniaxial tension until break. As the amount of curing

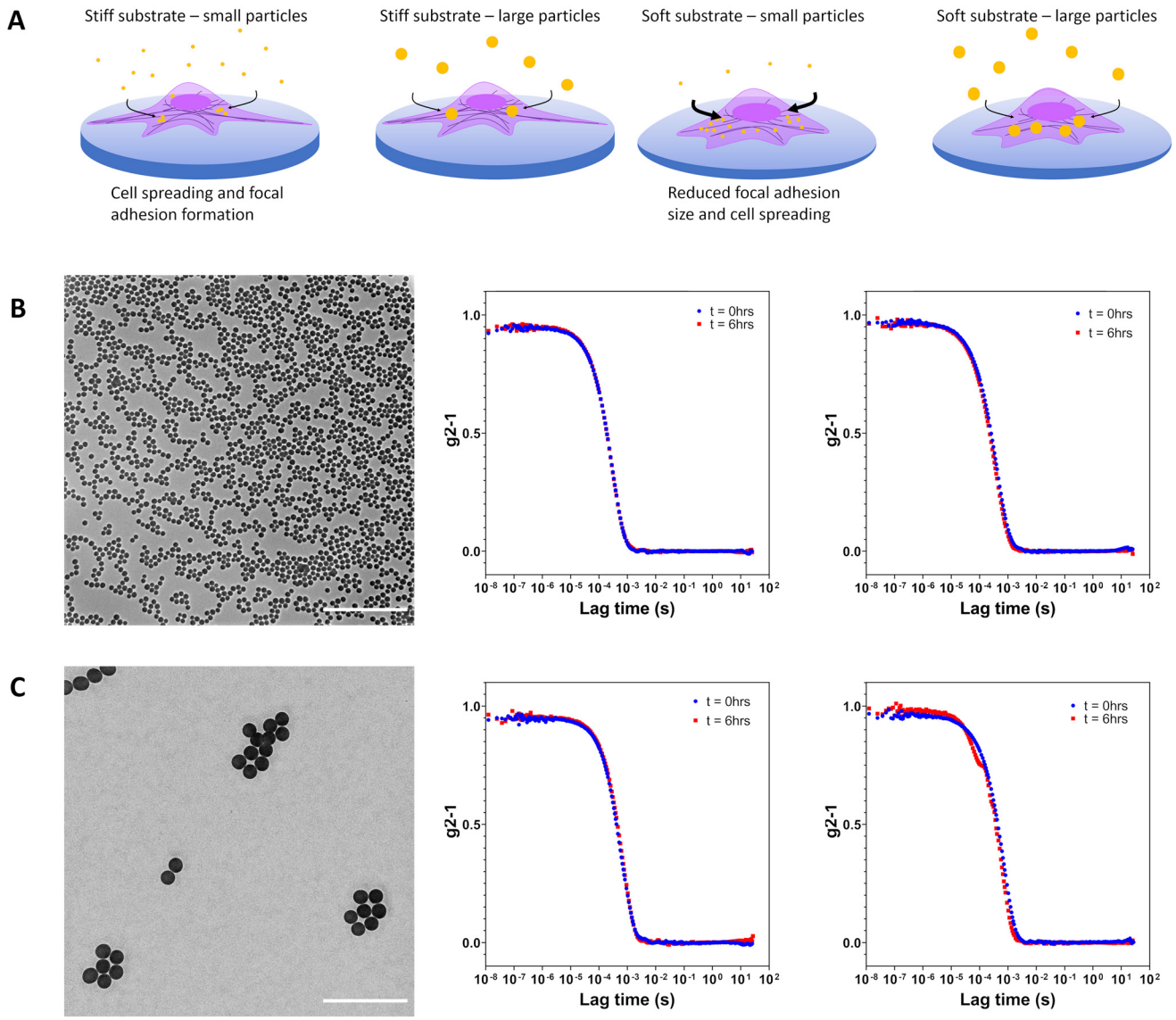

Fig. 1 (A) Schematic representation of the influence of substrate stiffness on cell endocytosis of 120 nm and 360 nm Cy5-labelled silica particles. Cell spreading and focal adhesion maturation on tissue culture polystyrene is abrogated when cultures are performed on softer fibronectin-coated PDMS 10 : 1 and fibronectin-coated PDMS 40 : 1. Increased internalization of particles was observed for cells on more mechanically compliant substrates. (B) Transmission electron micrograph of silica nanoparticles (d_{TEM} = 120 nm). Corrected time course dynamic light scattering measurements performed in water and supplemented RPMI at 0 h and 6 h indicate particle stability. (C) Transmission electron micrograph of silica particles (d_{TEM} = 360 nm). Corrected time course dynamic light scattering measurements performed in water and supplemented RPMI at 0 h and 6 h indicate no particle aggregation. Scale bars represent 2 μm.

agent was reduced, the Young's modulus was found to decrease from 2.7 MPa to 130 kPa while the strain to break increased from 0.9 to 2.1 (Fig. S3, ESI†). This lower Young's modulus is closer to the mechanical response of physiological tissue than that of standard tissue culture plastic which is typically in the range of 1 GPa.[31] Furthermore, the Young's modulus of tissues in lung fibrosis and cancer are approximately 100 kPa.[32,33]

PDMS surfaces were rendered better suited to cell culture by first coating them with fibronectin, a commonly found protein in native extracellular matrix.[34] As shown by Toworfe *et al.*, plasma activation of PDMS can improve fibronectin adhesion and support cell growth for up to 72 hours.[35] Surface water contact angle measurements were performed in order to assess the potential impact of hydrophobicity on cell behaviour. In comparison to sterile glass, fibronectin-coated PDMS (10 : 1, 40 : 1) had markedly higher hydrophobicity, 43° compared with 92° and 103°, respectively (Fig. S4, ESI†). The biocompatibility of the substrates was examined for both A549 and J774A.1 in contact with culture surfaces and with particles in suspension at 20 μg mL^{-1}. No cytotoxic effects were measured based on release of lactate dehydrogenase as a result of compromised membrane integrity (Fig. S5, ESI†).

The role of mechanical properties of the cell substrates in the regulation of cell behaviour remains an overlooked aspect of nanoparticle endocytosis. Recent studies have indicated that mechanical priming can have profound consequences for particle interactions and uptake.[12,13,36–38] Generally, it had been observed that particle uptake was greater on stiffer substrates, whereby cells exhibited greater cell spreading and therefore a greater area through which particles could be internalized. It was noted that although particle uptake increased in the cells, the area normalised membrane flux was decreased as a consequence of higher membrane tension.[13] In addition to membrane tension, it has been argued that cell spreading and the resultant traction force generation increases the cell stress state which opposes particle uptake.[37] In this biophysical model for cellular control of endocytosis, by altering cell stress state, greater cellular uptake can be generated as membrane tension can be lowered while also increasing the exposed surface area of the cell. Learning how cell mechanics influence endocytosis can lead to novel approaches for optimizing particle–cell interactions.[39] We explore how spreading may impact the mechanoregulation of endocytosis in both phagocytic and non-phagocytic cells. Furthermore, we highlight a possible biological mechanism by which cells are able to integrate information related to cell spreading and stress state to regulate endocytic activity.

The impact of culture substrate stiffness on particle endocytosis was assessed in two distinct cell types, A549 and J774A.1 were seeded on substrates with differing mechanical properties (namely: glass, fibronectin-coated PDMS 10 : 1 on glass and fibronectin-coated PDMS 40 : 1 on glass). A549 are one of the most commonly used cell lines used in assessing particle interactions, while J774A.1 display key characteristics of macrophages such as phagocytosis.[23,25] Previous reports have highlighted how mechanical properties can influence a number of cell behaviours.[28,40,41] However, how substrate rigidity influences the interaction of cells with particles has been largely overlooked. By characterising the stiffness-dependent endocytic activity in these cells, an appreciation for cell-dependent behaviour which is mechanically contextualised, such as for cancer tissue, can be developed.

Adhesion of cells to a surface and their ability to spread was determined through phase contrast microscopy and fluorescence microscopy (Fig. 2a and b and Fig. S6, ESI†). Visualization of cell morphology by fluorescence microscopy was performed on identically prepared surfaces with the replacement of tissue culture plastic with sterile glass. Cell area was determined by staining F-actin which is a vital part of the cell cytoskeletal architecture and can reflect changes in mechanotransduction.[42] When A549 cells were cultured on substrates with differing stiffness, mean cell area decreased from 1560 μm^2 on glass to 1140 μm^2 on PDMS 10 : 1 and 1050 μm^2 on PDMS 40 : 1 (Fig. 2b and Table S2, ESI†). The reduction in cell surface area was accompanied by an increase in the aspect ratio from 1.4 to 1.6, indicating that cell spreading was restricted, resulting in spindle-like cell morphology (Fig. 2c).

Substrate stiffness influence on endocytosis was determined by measuring the median fluorescence intensity (MFI) of A549 cultured on TCPS or fibronectin-coated PDMS 10 : 1 and 40 : 1 following exposure to Cy5-labelled 120 nm and 360 nm silica particles at a concentration of 20 $\mu g\ mL^{-1}$ for six hours. Increasing particle internalization is expected to result in a proportional increase in fluorescence intensity. MFI was higher for cells cultured on softer PDMS substrates than on TCPS indicating more particle endocytosis in soft environments (Fig. 2d). Stiffness-dependent uptake was strongly correlated with particle size as smaller particles (120 nm) exhibited a 5.7-fold and 6.5-fold increase in MFI for PDMS 10 : 1 and 40 : 1, respectively. In contrast, while uptake of larger particles (360 nm) was also increased on soft substrates, the increase in MFI was only approximately 2.4-fold for PDMS 10 : 1 and 40 : 1. Differences observed in the uptake preferences of A549 indicate that substrate rigidity influences cell behaviour with softer environments resulting in increased particle endocytosis. Concordantly, Williams *et al.* had also found that particle uptake was enhanced in A549 when they were cultured on soft polyurethane substrates compared with stiffer membrane substrates and polyester transwell inserts, both submerged and at air–liquid interface conditions.[43] Unlike previous work by Wei *et al.*, A549 cells were found to have more particle uptake on soft rather than stiff substrates.[38] It is worth noting that the areal differences characterised by both Huang *et al.* and Wei *et al.* are more than three times greater on stiff substrates than on soft substrates.[13,38] This marked difference in cell area may explain why cell spreading induced by substrate stiffness has a stronger impact on particle uptake which increases with surface rigidity. While we observe differences in cell spreading, the distinction is less pronounced with stiff surfaces resulting in cells with an area which is only 1.5 times larger than soft surfaces. Upon examining the role of cell stress state on cellular uptake, Wei *et al.* identified that increased traction force and physical cell stress associated with cell spreading inhibit endocytosis.[37] Accordingly, changes to cell stress state may be exerting a dominant effect over cell area in facilitating the increase in particle uptake on softer surfaces.

Unlike non-phagocytic A549, phagocytic J774A.1 macrophages showed greater spreading on intermediate (PDMS 10 : 1, 648 μm^2) substrates than on stiff (glass, 378 μm^2) and soft (PDMS 40 : 1, 562 μm^2) surfaces (Fig. 2f and Table S3, ESI†). However, there was no difference in the cell aspect ratio across the surfaces. Notably, human macrophages have been shown to exhibit biphasic spreading behaviour on differently stiff substrates and this may reflect the roles of macrophages in mechanically distinct environments which provide cues to guide adhesion and migration behaviour.[44] In accordance with literature, culture of cells on softer substrates reduces spreading area of both A549 cells and can modulate macrophage spreading.[27,45] Differences in internalisation behaviour between A549 and J774A.1 reflect cell-dependent proclivities towards particle uptake. As a macrophage, J774A.1 are professional phagocytic cells and normally participate in removal of foreign material and debris, explaining the difference in

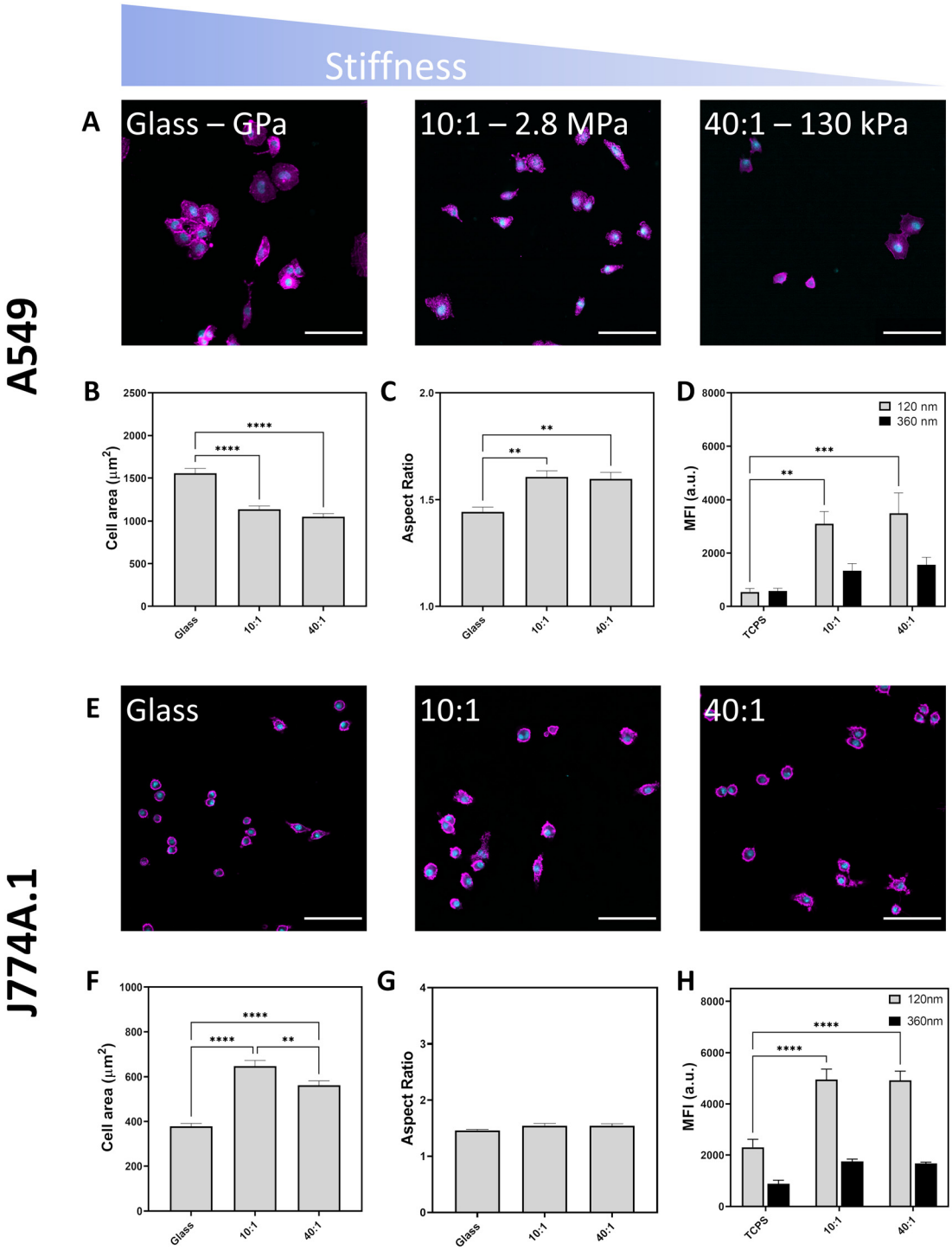

Fig. 2 Effect of substrate stiffness on cell morphology imaged by confocal laser scanning microscopy. Nuclei labelled in cyan and F-actin labelled in magenta. Scale bars represent 100 μm. (A) A549 attachment to glass, PDMS 10 : 1 and PDMS 40 : 1 following 24 hours of culture. (B) Cell area of A549 cultured on different substrates. (C) Aspect ratio of A549 cultured on mechanically distinct substrates. (D) Median fluorescence intensity of A549 cells upon exposure to fluorescent silica particles (120 nm and 360 nm) at a concentration of 20 μg mL^{-1} for six hours (E) light microscope images of J774A.1 cells showing their attachment and spreading on various surfaces. (F) Quantification of J774A.1 cell area on different substrates, (G) quantification of J774A.1 aspect ratio on different substrates. (H) Median fluorescent intensity of J774A.1 reflecting particle uptake *via* flow cytometry. All experiments performed with three biological replicates. Statistical significance determined by one-way ANOVA with Tukey's test, *$p < 0.05$, **$p < 0.01$, ***$p < 0.001$, ****$p < 0.0001$.

clearance behaviour with more uptake in J774A.1 than in A549.[25]

Particle uptake was also observed to be determined by substrate, with a doubling of MFI values for J774A.1 when cultured on softer PDMS for both 120 nm and 360 nm silica particles. The similar fold change in MFI values for both 120 nm and 360 nm particles suggests that mechanical effects are not size selective for macrophages. As a professional phagocyte, J774A.1 macrophage cells had higher MFI values than epithelial A549 due to an increased proclivity towards particle internalization.[25] Dissimilarly to A549, J774A.1 cells show no clear correlation between cell spreading and particle uptake, indicating that cell area is not the main contributor controlling their ability to internalize particles. Substrate stiffness has been shown to be able to co-regulate macrophage activity alongside soluble factors.[46] Patel *et al.* showed that RAW264.7 macrophages phagocytose more 2 μm IgG-coated latex beads when cultured on stiff gels. Conversely, Sridharan *et al.* found that THP-1 phagocytosed 1 μm fluorescent carboxylate-modified latex beads with the greatest efficiency on intermediate stiffness (88 kPa) gels. Summarily, while signalling based on the mechanical properties of the substrate material appear to be important regulators of particle uptake in macrophages, additional factors, such as polarization and phenotype are likely to be important considerations in governing internalization.

In our previous work, we had demonstrated that particles could adhere to surfaces and exert a local mechanoregulatory effect on cells.[12,18] Particles adsorbed onto a surface could be removed by cells and internalised in an actin-dependent manner between 12 and 24 hours of contact. The uptake of these surface particles is thought to occur through ventral or basolateral forces exerted by the cell.[18,47] Under physiological conditions, particles can adsorb to surfaces as well as components of the extracellular matrix. This attachment can lead to new interactions between particles and cells. Moreover, the particles can provide physical and topographical cues which can alter how cells subsequently interact with particles in their environment through co-exposure and competitive uptake. To understand the impact of the assembly of hard particles on a soft surface on mechanoregulation of endocytosis and whether co-exposure would highlight differences in uptake, we assembled negatively-charged silica particles on top of aminated PDMS surfaces (Fig. 3a, Table S1 ESI†). BDP-labelled silica was used, as a fluorophore with good discrimination against Cy5-labelled silica particles administered in suspension, to fabricate the particle-decorated surface (PD) by utilizing electrostatic interactions between negatively charged particles

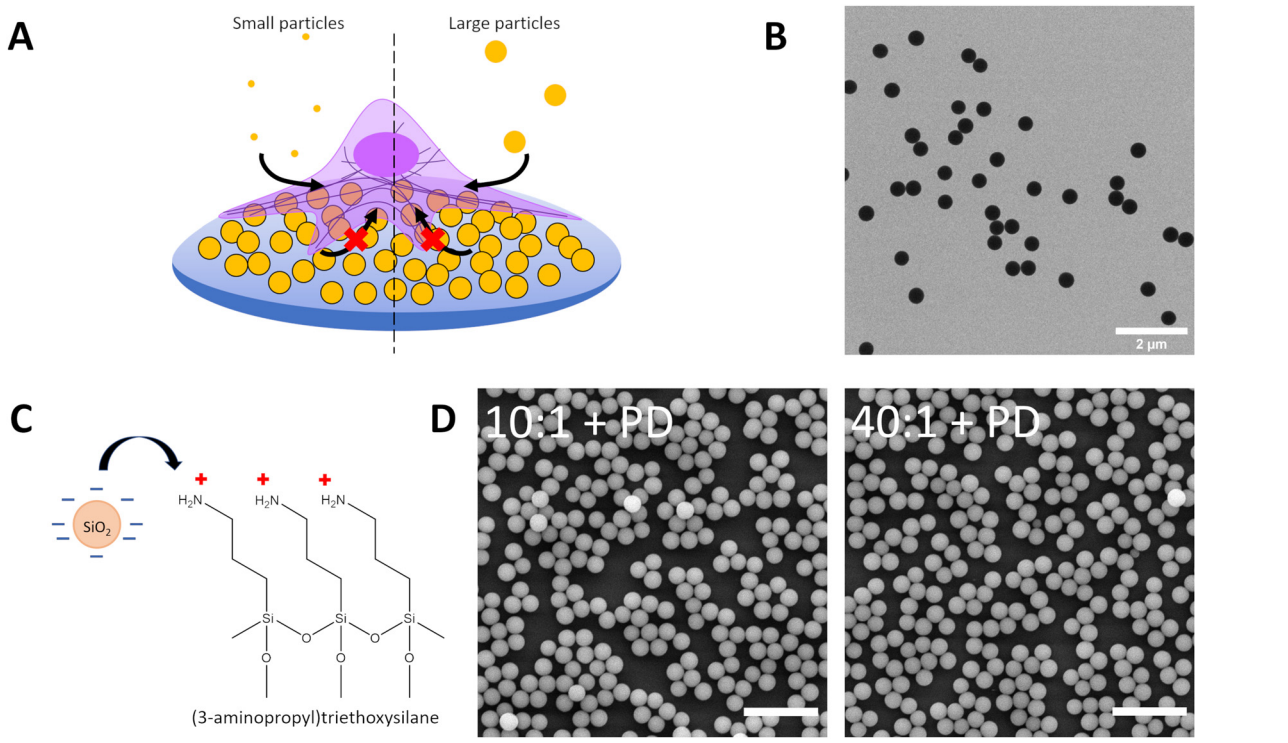

Fig. 3 (A) Schematic depicting uptake of small (120 nm) and large (360 nm) Cy5-labelled silica particles by A549 on particle-decorated substrates to assess the influence of particle-generated topography on particle internalisation in a competition co-exposure system. Particle-decorated substrates consist of 420 nm BDP-labelled silica electrostatically adsorbed to APTES-modified PDMS 10 : 1 (10 : 1 + PD) and APTES-modified PDMS 40 : 1 (40 : 1 + PD). (B) Transmission electron microscope image of silica particles (d_{TEM} = 420 nm) used to form the particle-decorated (PD). (C) Schematic of PDMS surface functionalization with 3-aminopropyltriethyoxysilane (APTES) to facilitate adsorption of negatively charged silica particles. (D) Scanning electron microscope image of PDMS 10 : 1 and PDMS 40 : 1 treated with APTES and decorated with silica particles (d_{TEM} = 420 nm) to form a particle-decorated surface. Scale bar represents 2 μm.

and positively charged (3-aminopropyl)triethoxysilane (APTES), resulting in a layer of silica particles attached on top of APTES-functionalised PDMS (Fig. 3b and c). The chemical modification of the surface with amines facilitated a more uniformly charged surface for controlled particle attachment, unlike proteins such as fibronectin which display variable surface chemistry as determined by the amino acid sequence.[48] Particle-decorated surfaces were visualised by scanning electron microscopy, showing that the production of a dense arrangement of particles in a monolayer configuration (Fig. 3d). By using BDP-labelled silica for the particle-decorated surface and Cy5-labelled silica for suspension, potential preferences between basal and apical uptake could be determined as well as changes in suspension-based uptake following signalling arising due to the effect of adsorption of particles to a surface and topography generation.

Cells were able to attach and adhere to particle-decorated (PD) modified PDMS surfaces consisting of 420 nm BDP-labelled silica particles which are electrostatically assembled on APTES-modified PDMS with a curing ratio of 10 : 1 or 40 : 1 (Fig. 4a and b and Fig. S7, ESI†). Over the culture period, little to no internalization of the surface particles was noted, with background fluorescence values similar for cells cultured on fibronectin-coated PDMS (Fig. S8, ESI†). The limited ability of cells to clear electrostatically adsorbed particles is indicative that substrate properties likely play an important role in particle–surface interactions and surface-mediated clearance.[12,18,49] Spreading of A549 on particle-decorated surfaces (10 : 1 + PD, 40 : 1 + PD) is notably reduced compared with fibronectin-coated PDMS and glass with the mean cell spreading area being 800 μm^2 for 10 : 1 + PD and 920 μm^2 for 40 : 1 + PD (Table S4, ESI†). In addition, cells display an increase in aspect ratio from 1.4 on glass to 1.7 on particle-decorated surfaces. As observed between human monocyte-derived macrophages (hMDMs) and a poly(*N*-isopropylacrylamide) (pNIPAM) particle-decorated surface assembled with the aid of APTES, minimal surface removal was present.[12] Cell spreading on particle-decorated surfaces was notably decreased which suggests that surface properties influence physical regulation of cell morphology.

Particle uptake for 120 nm and 360 nm Cy5-labelled silica were determined for A549 cultured on TCPS, 420 nm BDP-labelled silica particles on APTES–PDMS 10 : 1 (10 : 1 + PD) and 420 nm BDP-labelled silica particles on APTES–PDMS 40 : 1 (40 : 1 + PD) (Fig. 4c). Internalization of 120 nm silica particles increased 1.8-fold and 2.6-fold for 10 : 1 + PD and 40 : 1 + PD, respectively. Similarly, for 360 nm silica particles, MFI was higher by 1.7-fold and 2.3-fold on 10 : 1 + PD and 40 : 1 + PD substrates than on TCPS. The addition of hard silica particles to the surface of PDMS 10 : 1 and PDMS 40 : 1 is shown to attenuate the increase in particle internalization. Consequently, the contributions of particles to the local topography of the substrate are sufficient to give rise to a different cell stress state. The relative reduction in particle uptake between PDMS and particle-decorated PDMS suggests that the particles are partially shielding the softness of the underlying surface. Additional cues provided by particle topography may also contribute to the observed response. Although not directly assessed within the current study, the possibility of uptake competition between the apical and basal surfaces may lead to additional interactions that confer salient mechanical cues towards consequent cell decision making.

As an additional means of understanding substrate-induced changes in particle endocytosis, fluorescence intensity values obtained from flow cytometry experiments were normalised against cell spreading on each substrate (Fig. S9†). From Wei *et al.*, cell stress increases with substrate stress.[37] Following normalisation, our results indicate that for both A549 and J774, particle uptake increases with decreasing substrate stiffness and cell stress. A549 show a greater increase in particle uptake for 120 nm sized particles, while for 360 nm sized particles, the increase was similar across substrates. Contrastingly, uptake in J774 showed a tendency to increase with decreasing substrate stiffness without significant size-dependent behaviour. Together, these results are indicative

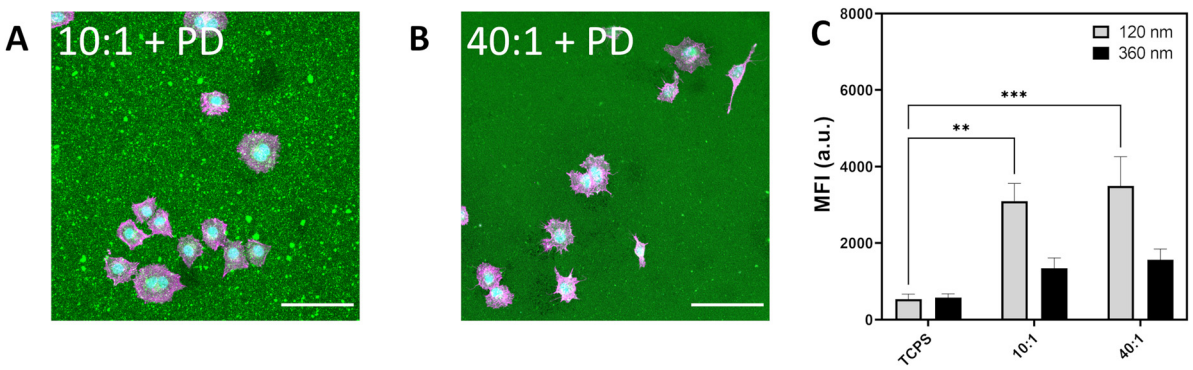

Fig. 4 (A) Light microscope image depicting A549 spreading on PDMS 10 : 1 decorated with silica particles. (B) A549 spreading on silica decorated PDMS 40 : 1. F-actin labelled in magenta, nuclei labelled in cyan and silica particle-decorated PDMS (BDP, 420 nm) in green. Scale bar represents 100 μm. (C) Median fluorescence intensity of A549 cultured on silica decorated PDMS showing uptake of Cy5-labelled silica 120 nm and 360 nm exposed for 6 h at 20 μg mL^{-1}. Data expressed as mean + standard error of the mean. Statistical significance determined by one-way ANOVA with Tukey *post hoc* test for multiple comparisons. *$p < 0.05$.

that decreasing substrate stiffness and likely cell stress are related to the observed changes in endocytosis in both cell types.[13,37] Interestingly, particle rigidity has been found to modulate lysosomal processing time, and it has been postulated that mechanical reciprocity would lead more deformable cells which can favour uptake of particles.[50] The sensitivity of cells to both particle and substrate stiffness may be suggestive of convergent or overlapping cellular pathways linking the physical environment and cues to mechanoresponsive output.

Mechanical cues present in the cellular microenvironment are sensed by a number of pathways and include the formation of focal adhesion plaques. Focal adhesions are complex assemblies of proteins which allow the cell to exert traction forces and participate in conveying substrate mechanical properties such as compliance to direct cell activity.[42] Visualization of focal adhesions is typically achieved by immunolabelling of marker proteins such as paxillin.[51] The area and length of the resultant focal adhesion plaques was reduced in A549 cultured on intermediate and soft substrates from 1.6 μm^2 on glass to 1.3 μm^2 and 1.5 μm^2 on PDMS 10 : 1 and PDMS 40 : 1, respectively (Fig. 5a–c and f, Table 1 and Table S4, ESI†). Focal adhesion size is also reduced on particle-decorated surfaces; 1.4 μm^2 and 1.0 μm^2 for 10 : 1 + PD and 40 : 1 + PD respectively (Fig. 5d–f). In contrast with previous particle-decorated surfaces, the assembly of 420 nm silica particles on aminated PDMS does not promote the maturation and enlargement of focal adhesion structures.[18] Arguably, the softer surface underlying the particles should hinder the development of traction forces through mechanical relaxation, leading to mixed surface mechanical characteristics. Curiously, when cultured on particle-decorated surfaces, the aspect ratio of focal adhesions was determined to have increased from 1.66 on PDMS 10 : 1 to 1.71 on PDMS 10 : 1 + PD and from 1.62 on PDMS 40 : 1 to 1.76 on PDMS 40 : 1 + PD (ESI Table S4†). Despite possessing a smaller total area, the higher aspect ratio focal adhesion plaques present on particle-decorated surfaces suggest that topography associated with the substrate helps to induce filopodal and lamellipodal formation.

Table 1 Summary of focal adhesion characteristics for A549 cultured on different surfaces for 24 h

	Area (μm^2)	Length (μm)	Aspect ratio	No. cells
Glass	1.62 ± 0.02	1.89 ± 0.01	1.69	172
10 : 1	1.26 ± 0.02	1.66 ± 0.02	1.66	113
40 : 1	1.47 ± 0.02	1.77 ± 0.01	1.62	135
10 : 1 + PD	1.40 ± 0.04	1.81 ± 0.03	1.71	122
40 : 1 + PD	0.99 ± 0.02	1.47 ± 0.02	1.76	130

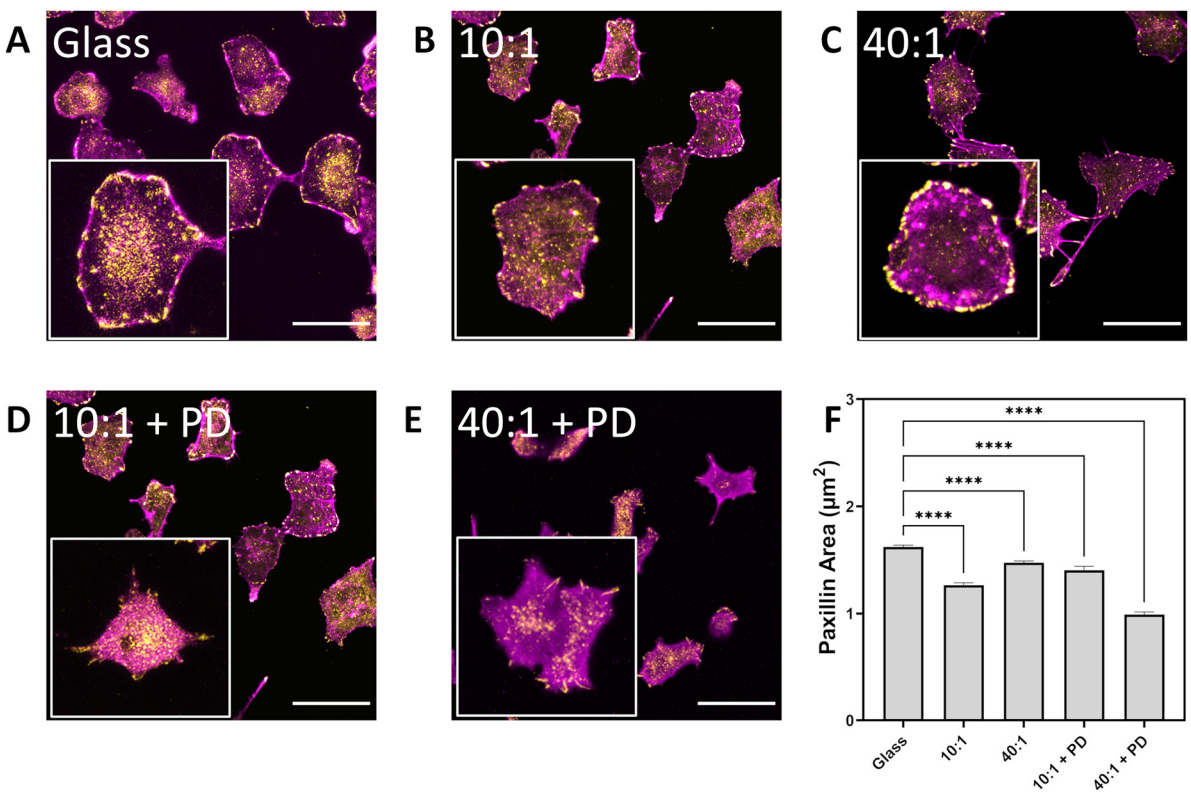

Fig. 5 Effect of substrate stiffness and topography on formation of focal adhesion plaques as determined by paxillin labelling and visualization by confocal laser scanning microscopy. A549 on (A) glass, (B) PDMS 10 : 1, (C) PDMS 40 : 1, (D) PDMS 10 : 1 + PD, (E) PDMS 40 : 1 + PD. F-actin labelled in magenta while paxillin is labelled with rabbit anti-paxillin and goat anti-rabbit IgG conjugated with AlexaFluor 555 in yellow. Scale bar represents 50 μm. (F) Paxillin area assessed over $n > 100$ cells over three biological replicates. Data expressed as mean + sem. Statistical analysis performed using a one-way ANOVA with Tukey's *post hoc* test, *****$p < 0.0001$. PD – particle-decorated surface.

Emerging evidence suggests that mechanoregulation of particle uptake primarily occurs through changes in clathrin and caveolae-mediated endocytosis.[38] A549 are able to internalize particles through clathrin and caveolae-mediated pathways as well as macropinocytosis while also being able to exert strong traction forces.[18,52] Moreover, A549 exhibit stiffness-dependent focal adhesion maturation and cell spreading as well as YAP expression to facilitate a better understanding of the relationship between mechanoregulatory networks and endocytosis.[28,53] YAP appears to regulate cytoskeletal dynamics, acting downstream of changes in integrin and focal adhesion assembly, as well as in cadherin and Wnt signalling.[54,55] Recent work has indicated that YAP has been shown to exert transcriptional control over caveolin and provides a potential link between mechanosensing of physical cues such as stiffness and topography through integrin/adhesion machinery and mechanoregulation of endocytosis.[56]

YAP expression was assayed by western blot to determine if there is a correlation with substrate-induced changes in endocytosis. Expression of YAP was found to be significantly upregulated on PDMS 10 : 1 and PDMS 40 : 1 with an increase of 1.9-fold and 2.2-fold, respectively (Fig. 6). In comparison, the increase in YAP expression was found to be marginally greater at 1.4-fold and 1.7-fold for PDMS 10 : 1 + PD and PDMS 40 : 1 + PD. Remarkably, the expression pattern of YAP in cells on different substrates mirrors the pattern of endocytosis of small particles with the greatest upregulation of expression occurring on PDMS 10 : 1 and PDMS 40 : 1. Moreover, a similar pattern is also observed for the particle-decorated surfaces. The positive correlation between YAP expression and endocytic trends is suggestive that the mechanosensitivity of YAP facilitates mechanically-driven regulation of endocytosis and particle uptake. As YAP/TAZ are essential for the expression of CAVIN1 and CAVEOLIN1, it provides a potential link between mechanosensing and regulation of endocytic machinery.[57,58]

YAP is an important signalling component in the Hippo pathway and is responsive to changes in the physical microenvironment.[54] Signalling of mechanical information to the cell is mediated by cellular structures such as focal adhesions, caveolae and clathrin-coated pits which respond to cell and membrane stress. Observed alterations in focal adhesion size and morphology arising from the stiffness and topography of the substrate are expected to alter mechanobiological signaling.[59,60] YAP is able to respond to changes in cytoskeletal stress associated with focal adhesion maturation and can exert feedback actions by regulating their assembly and turnover.[61] In a monolayer wound model, Mason *et al.* detected an increase in total YAP expression in migrating cells ahead of the wound edge.[62] Similarly, depletion of YAP reduced the ability of cells to persistently migrate as well as increasing cell stress which was accompanied by maturation and stabilization of larger focal adhesions. Notably, overexpression of YAP in cells on soft substrates would be explain the observed reduction in focal adhesions and a reduced cell stress state that would promote endocytosis consistent with observations by Wei *et al.*[37]

In addition to its role in cytoskeletal feedback and turnover dynamics related to focal adhesion and actin filament assembly, YAP may also interact with key endocytic components such as clathrin and caveolin. Clathrin mediates the endocytosis of many particles and the lifetime of clathrin structures on the cell membrane is influenced by membrane tension and cell spreading.[63] Under conditions where membrane and cell tension is high, clathrin-coated pits exhibited shorter lifetimes, which was attributed to abortive assembly and turnover. Caveolin-1 has also been demonstrated to be involved in facilitating nanoparticle internalization as well as regulating YAP mechanotransduction.[64,65] The transcriptional control of caveolin-1 expression and its negative feedback actions on YAP highlight an additional mechanism through which substrate stiffness may modulate endocytic activity. Additionally, YAP

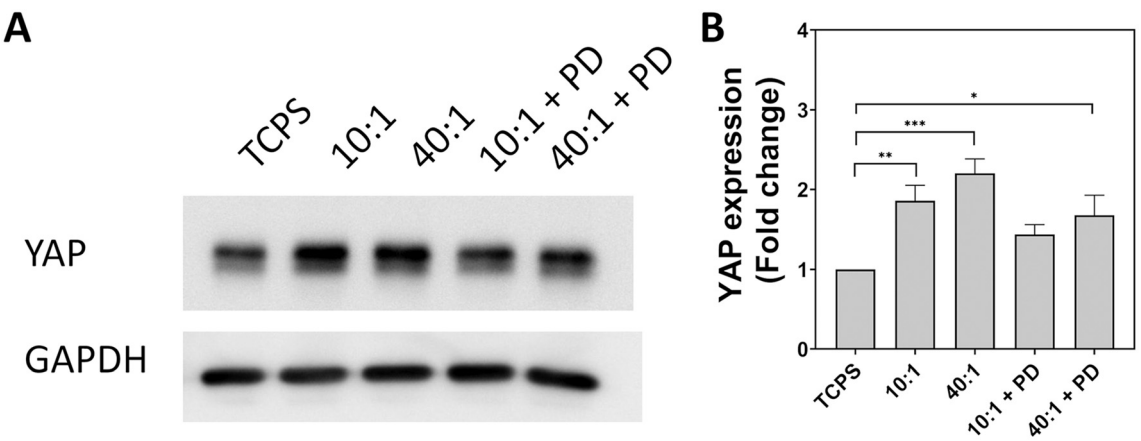

Fig. 6 Evaluation of YAP expression in A549 cells cultured for 24 hours on substrates with different stiffness and topography. (A) Bands obtained from western blot for YAP and GAPDH. GAPDH used as a loading control. (B) Fold change in YAP expression expressed as mean + standard error of the mean from three biologically independent replicates. Statistical significance determined by one-way ANOVA with Tukey's *post hoc* test. *p < 0.05, **p < 0.01, ***p < 0.001. TCPS – tissue cell culture plastic. PD – particle-decorated.

can also promote macropinocytosis for the entry of larger particles.[58] Interestingly, Wei *et al.* showed in a western blot analysis, an increase in A549 expression of both clathrin and caveolin-1 on stiff gels. Moreover, inhibition of clathrin and caveolin-mediated endocytosis abrogated stiffness-mediated effects on endocytosis. Our observation that YAP expression is increased on soft substrates for A549 and corresponding increase in endocytosis suggests that mechanical cues regulate particle uptake through YAP, which can consequently control caveolin-1 expression. YAP control of cytoskeletal dynamics which define cell rigidity also explain how reducing cell stress was able to increase particle uptake in HCT-8 cells.[37]

Elevated YAP levels have been noted in A549 tumour spheres and may be responsible for conferring cancer stem cell qualities that has been clinically shown to contribute to poor prognosis in non-small cell lung cancer.[53,66,67] It is particularly significant as the increased metastatic potential is facilitated by actin and focal adhesion turnover.[62] Taken holistically, YAP tends to drive cell division and cell-cycle progression.[68] Alongside improved cell survivability, previous literature suggests that YAP supports actin reorganisation for movement and migration and would understandably facilitate increased nutrient uptake required for growth and division. A potential route for YAP to exert transcriptional control over caveolin would provide a mechanism through which cells could sense their physical environment, modulate focal adhesions and regulate endocytosis.[57,59] The interplay between the mechanical properties of the local environment, cell mechanics and protein interactions allows a cell to integrate information from its environment and balance the biophysical requirements of cell movement and plasma membrane perturbation. A possible force balance between endocytosis and adhesion was posited by Baschieri *et al.* and is consistent with our observations regarding how perturbations in adhesion through substrate engineering alter YAP expression and resultant trends in particle internalisation.[69] As both clathrin and caveolin-based endocytic structures have been associated with adhesion processes,[70] further elucidation of pathway interactions and crosstalk is critical to understanding how regulation of adhesion and associated signalling occurs, how cells regulate endocytosis, and how cells integrate information from these two systems through cytoskeletal dynamics. Due to the number of interactions associated with YAP, it may be possible to fine tune its actions through mechanotargeting to enhance the efficacy of particles used in nanomedicine.

Understanding endocytosis is vital to evaluation of the impact of exogenous particles on cells as well as predicting the efficacy of nanomedicines. However, the contributions of the microenvironment are difficult to mimic in cell culture assays. Given the wide array of unique niches which are present in development, homeostasis and pathological progression, characterization of cellular interactions requires consideration of the most salient features and their reproduction. Replication of physical factors can aid in model design as they may alter cellular rates of endocytosis following crosstalk with mechanosensitive pathways and manifests in organization and the dynamic behaviour of the cytoskeletal network. Cancers may be particularly challenging to model due to dysregulation of normal cellular functions and the presence of harsh environmental cues including low oxygen and nutrient availability. Importantly, many of the pathological changes which occur during cancer progression as well as during other disease states such as fibrosis, involve the production of extracellular matrix and corresponding feedback which can drive further aberrant behaviour through improper mechanotransduction. Similarly, exposure to particles can generate their own biophysical cues that have repercussions for fundamental processes such as cell attachment, adhesion and migration. Correcting mechanosignalling pathways may offer a powerful method for overcoming current limitations in treatment efficacy as well as a greater appreciation for the likely biological outcomes given certain physical cues such as stiffness and topography and their consequent bearing on cell phenotype and behaviour. Notably, physical cues present the in the microenvironment, such as those generated by particles, define the state of cell mechanics in terms of cytoskeletal organization and adhesion. Cytoskeletal turnover related to adhesion also affects the regulation of endocytic processes and results in physical control of particle internalization which is defined by cell type.

Conclusions

Mechanical features in the cellular environment dynamically control biological activity mediated through the interplay of membrane tension, integrins, focal adhesions, cytoskeletal organization and transcriptional regulators. The centrality of cell mechanics in defining and reflecting cell behaviour is becoming more apparent and a deeper appreciation of how these cues interact and effect signalling pathways is necessary. Softer substrates promoted particle uptake in both epithelial cells and macrophages, with epithelial spreading reduced by soft materials. Internalization of small 120 nm sized silica particles into A549 was more strongly influenced by mechanical effects than that of 360 nm silica particles, with an increase of 6.5-fold compared with exposures performed on standard culture plastic. Coating soft substrates with hard particles alters mechanical signalling and consequently partially masks the properties of the underlying surface, resulting in only a 2.6-fold increase in 120 nm silica particles by A549. As endocytosis and vesicle trafficking are contingent on actin polymerization, changes to cell mechanics have a corresponding impact on particle uptake. Changes to actin and cytoskeletal organization have been linked to YAP activity, YAP expression was found to increase in A549 by up to 2.2-fold on PDMS 40 : 1 which correlated with the greatest increase in particle internalization. Further work is needed to elaborate on its role in pathway crosstalk related to endocytosis and identify if specific actions of YAP can be selectively enhanced or suppressed to improve susceptibility of cancer to treatment or augment tissue regeneration and engineering.

Materials and methods

Synthesis of silica particles

Dye-labelled silica particles were produced by adapting the Stöber method.[71] Labelling of silica particles with dye was achieved by reacting a *N*-hydroxysuccinimide (NHS) ester bearing fluorescent dye with an amine-terminated organosilane (APTES). 2.3 mg of sulfo-cyanine5 (Cy5) NHS ester (Lumiprobe, Germany) was dissolved in 200 μL dimethylsulfoxide (DMSO) (>99.9%, sterile-filtered, Sigma Aldrich, Germany) to which 3 μL of (3-aminopropyl)triethoxysilane (APTES) (99%, Sigma Aldrich, Germany) was added and allowed to react overnight. For small (120 nm) silica particles, 29 mL H_2O, 81 mL ethanol (>99.8%, analytical grade, VWR, United Kingdom) and 2.9 mL of ammonia solution (25% for analysis, Merck, Germany) were mixed in a reflux condenser and heated to 60 °C. Subsequently 10 mL of tetraethylorthosilicate (TEOS) (>99.0%, Sigma Aldrich, Germany) was added and stirred for two minutes after which 200 μL of Cy5–APTES was added and the mixture was allowed to react for five hours. The suspension was centrifuged three times at 2000*g* for 40 minutes and dispersed in ultrapure water. Large (360 nm) silica particles labelled with Cy5 were prepared with 13.5 mL H_2O, 174 mL ethanol and 45 mL ammonia solution were heated to 60 °C. Following, 22.5 mL of TEOS was added to the reaction vessel and reacted for two minutes prior to the addition of the dye-conjugated silane and reacted for three hours before three centrifugation cycles at 2000*g* for 20 minutes and redispersion in ultrapure water. Green BODIPY fluorescent dye NHS ester (BDP) (Lumiprobe, Germany) was conjugated to APTES overnight in DMSO. BDP-labelled silica was prepared by mixing 13.5 mL H_2O, 174 mL ethanol and 40.9 mL ammonia solution. The reaction mixture was brought to 55 °C and equilibrated for 30 minutes. Then, 22.5 mL of TEOS was added and stirred for three minutes, before addition of 200 μL of BDP–APTES. Mixture was allowed to react for three hours followed by three centrifugation cycles at 2000*g* for 20 minutes each.

Particle characterization

Synthesised silica particles were characterised by performing dynamic light scattering and zeta potential measurements with a Brookhaven 90Plus Particle Size Analyzer with phase-amplitude light scattering (PALS) (Brookhaven Instruments, USA) with a 40 mW diode laser, λ = 635 nm. Hydrodynamic diameter and polydispersity were determined for dilute suspensions with a scattering angle of 90° at 25 °C.

Particles were visualised by transmission electron microscopy to validate size and morphology. A dilute suspension was drop cast onto a Formvar-coated copper 300 square mesh TEM grid coated with carbon film (Electron Microscopy Sciences, USA) and allowed to dry overnight at room temperature. Images were acquired with a Tecnai Spirit transmission electron microscope equipped with a 120 kV LaB_6 filament and a 2048 × 2048 pixel wide angle Veleta camera. Particle size distribution was determined by thresholding and binarization of micrographs followed by automated analysis in Fiji (ImageJ, USA). Mean diameter and standard deviation were determined after counting at least 500 particles.

Colloidal stability of Cy5-labelled particles was determined by collecting scattering intensity autocorrelation functions in a DLS spectrometer (LS Instruments, Switzerland) at a scattering angle of 90° at 37 °C at 0 h and 6 h of incubation in either ultrapure water or serum supplemented cell culture medium at a concentration of 100 μg mL^{-1}. Correlograms were corrected to remove the effect of protein in culture medium.[72]

Colloidal stability was also assessed using a Malvern Zetasizer Nano (Malvern Panalytical, UK), operating at a scattering angle of 173°, at a concentration of 100 μg mL^{-1} at 37 °C either at 0 h and 6 h. Intensity-weighted size distributions were produced using non-negative least squares regression (Multiple Narrow Modes).

Mechanical characterization

Mechanical characterization of cured polydimethylsiloxane (PDMS) Sylgard 184 (Dow Corning, USA) formulations was performed with a ZwickRoell Z010 tensile tester following ASTM D638. Cast PDMS was cut to specifications using a dumbbell press with a nominal width and thickness of 5 mm and 2.5 mm, respectively, gauge length for tests was approximately 22 mm. Tests were conducted at room temperature at a strain rate of 50 mm min^{-1} until break. Tensile data is expressed as mean ± standard deviation.

Water contact angle

Water contact angle measurements were obtained through the sessile drop method on glass and modified PDMS surfaces. 3 μL of water was dispensed and contact angle measurements were captured using an OCA15 Pro goniometer (DataPhysics Instruments, Germany). Five measurements were conducted for each sample, data presented as mean ± standard deviation.

Cell culture

Human alveolar type II epithelial cells (A549) and murine macrophage cell line (J774A.1) were purchased from the American Type Cell Culture Collection (ATCC, USA). Cells were cultured and maintained in Roswell Park Memorial Institute 1640 (RPMI-1640, Gibco, Switzerland) supplemented with 10% foetal bovine serum, 1% penicillin/streptomycin and 1% glutamine. Cells were kept at 37 °C, 5% CO_2 and 95% relative humidity and passaged between 80–90% confluency.

Cytotoxicity

Cytotoxicity caused by either the substrate materials or the particles used were assessed by collecting culture supernatant and determining L-lactate dehydrogenase (LDH) activity according to manufacturer's protocol (Roche, Germany) for A549 and J774A.1 cells. LDH release associated with compromised cell membrane integrity was measured through production of formazan detected spectrophotometrically (Benchmark microplate reader, BioRad, Switzerland) at 490 nm with a reference wavelength of 630 nm. Triton-X was applied as a positive control at 0.2% v/v for at least 30 minutes. Values were

obtained for three biologically independent replicates and presented as mean ± standard error of the mean.

Particle uptake experiments

PDMS (Sylgard 184, Dow Corning, USA) was prepared at either 10 : 1 or 40 : 1 curing ratio (base elastomer to curing agent, g g^{-1}) and added to a six well plate and cured for two hours at 70 °C. Surfaces were activated by exposure to one minute of plasma and incubated with 10 μg mL^{-1} human fibronectin (>90% by SDS-PAGE, Corning, USA) in PBS for two hours and rinsed. An untreated tissue culture polystyrene well was used to assess cell behaviour on stiff culture substrates. A549 and J774A.1 cells between passages 4–20, were seeded on surfaces at a density of 5×10^6 cells per well and cultured for 18 hours. A suspension of Cy5-labelled silica particles was added in serum-supplemented medium at a concentration of 20 μg mL^{-1} and incubated for a further six hours.

Particle-decorated PDMS were prepared by preparing and curing PDMS at either 10 : 1 or 40 : 1. Cured PDMS 10 : 1 or PDMS 40 : 1 was exposed to plasma for one minute and immersed in 2% v/v APTES in ethanol for two hours. APTES-treated surfaces were rinsed with ethanol and water prior to the addition of a suspension of silica particles labelled with BDP at a concentration of 5 mg mL^{-1} for one hour. Surfaces were gently rinsed to remove unattached particles at least ten times with ultrapure water. A549 cells between passages 4–20 were seeded on surfaces at a density of 5×10^6 cells per well and cultured for 18 hours. Cy5-labelled silica particles were added at a concentration of 20 μg mL^{-1} and incubated for six hours.

After particle exposure, A549 cells were detached by trypsinization by addition of trypsin–EDTA (200 μL) for 5 min followed by the addition of 800 μL of supplemented RPMI. Cells were centrifuged at 4 °C for 5 min at 300*g*, and resuspended in PBS. A second centrifugation was conducted, followed by cell resuspension in flow cytometry (FC) buffer (PBS with 1% w/v bovine serum albumin (BSA) (Sigma-Aldrich, USA), 0.1% v/v sodium azide (Sigma-Aldrich, USA) and 1 mM ethylenediaminetetraacetic acid (EDTA) (Sigma-Aldrich, USA) at pH 7.4). J774A.1 were scraped off in 1 mL of PBS, using a cell scraper (Sarstedt, USA) and collected in a flow cytometry tube (Corning, Falcon®, 5 mL Polystyrene Round-Bottom Tube, Switzerland). Cells were centrifuged at 4 °C for 5 min at 300*g*, and resuspended in cold FC buffer. Data acquisition was performed on a BD LSR FORTESSA (BD Biosciences, USA) where 20 000–30 000 events were recorded. Flow cytometry data was analysed using the FlowJo software v.10.7.1.

Quantification of cell spreading

The spreading of cells on different substrates was assessed by fluorescence microscopy. Cells were seeded at 200 000 cells per dish in MatTek sterile glass bottom dishes (MatTek, USA) where surfaces were produced by spin coating PDMS at 2000 rpm for two minutes and curing. PDMS surface functionalization was performed by exposure to plasma for one minute and immersion in 10 μg mL^{-1} fibronectin or 2% APTES in ethanol. Cells were cultured in serum supplemented medium for 24 h before being washed twice with PBS (Gibco, Switzerland) and fixed with 4% *para*-formaldehyde in PBS. Nuclei and cytoskeleton were stained with 4′,6′-diamidino-2-phenylindole (DAPI, Switzerland) and rhodamine phalloidin (Thermo Fisher, Switzerland), respectively. Images were acquired with a Zeiss LSM 710 (Zeiss, Germany) confocal laser scanning inverted microscope using a 20× (numerical aperture 0.8) lens. Fluorophores were excited sequentially and collected with a field of view of 425.10 μm × 425.10 μm with a pixel density of 1024 × 1024 and a pixel dwell time of 1.28 μs. Images were processed with a Mathematica script as described by Antonetta.[73] Data are shown as mean + standard error of the mean for $n > 100$ cells. A parametric one-way analysis of variance (ANOVA) was performed with Tukey's multiple comparisons test to compare significance of effects. Values were considered significant (*) if $p < 0.05$.

Quantification of paxillin size

Focal adhesion size was quantified by image processing in Fiji. Cells were seeded at 200 000 cells per dish in MatTek sterile glass bottom dishes on glass and functionalised PDMS surfaces for 24 h followed by fixation. Cells were fixed with 4% paraformaldehyde in PBS and blocked with 0.1 M glycine solution. Permeabilization was performed with 0.1% Triton X and blocked with 1% BSA. Primary monoclonal rabbit anti-paxillin antibody (1 : 200) (Abcam, UK) was incubated at 37 °C for two hours and incubated with goat anti-rabbit secondary antibody conjugated with AlexaFluor 555 (1 : 200) (Abcam, UK) for one hour. F-actin was subsequently labelled with AlexaFluor 647 phalloidin (Thermo Fisher, Switzerland). Preparations made in 1× PBS (Carl Roth, Germany). Image processing was performed following the step by step method outlined by Horzum.[51] Area, Feret length and aspect ratio obtained with ImageJ. Data is shown as the mean + standard error of the mean for $n > 100$ cells. An ANOVA was performed to compare values, which were considered significant (*) if $p < 0.05$.

Western blot

Total protein was isolated from A549 cells seeded on substrates for 24 hours in six well plates with 5×10^6 cells seeded per well. Cell lysis was performed directly in the wells by adding 120 μL of ice-cold M-PER buffer (Cat. # 78501, Thermo Scientific) supplemented with Halt™ Protease Inhibitor Cocktail, EDTA-free (Cat. # 78425, Thermo Scientific). Plates were kept at 4 °C for 20 min. Protein lysates were pipetted up and down, transferred to 1.5 mL Eppendorf tubes, kept on ice for 10 min and centrifuged at 14 000*g* for 5 min. The protein in the supernatant was collected and measured spectrophotometrically (Thermo Scientific™ NanoDrop™ 2000 Spectrophotometer) at the wavelength of 280 nm using bovine serum albumin (BSA) as the standard. The samples were boiled in a reducing Laemmli buffer for 5 min, and the same amount of protein was loaded in a 7.5% SDS-PAGE (Bio-Rad, Hercules, USA). Proteins were electrophoretically transferred onto polyvinylidene difluoride (PVDF) membranes at 150 mA

for 75 min under wet conditions. A solution of 0.1% w/v Ponceau S (Cat. # 141194, Sigma-Aldrich, Switzerland) was used to confirm the transfer of proteins. A solution containing 3% w/v BSA and 0.1% v/v Tween 20 (Cat. # P9416, Sigma-Aldrich, Switzerland) in Tris-buffered saline (TBS) solution was used to block the nonspecific sites for one hour. The same solution was used for immunostaining with primary and secondary antibodies. Three rounds of washing with Tween-Tris-buffered saline (TTBS) (0.1% v/v Tween 20 in TBS) were performed between steps. Primary antibody was added to the blots overnight at 4 °C. The following concentrations of antibodies were used: anti-glyceraldehyde-3-phosphate dehydrogenase (GAPDH) (1 μg ml^{-1}, sc-47724, Santa Cruz Technology, USA), anti-YAP (1 μg ml^{-1}, Cat. # 14074, Cell signaling, UK). The blots were then incubated with a goat anti-mouse horseradish peroxidase (HRP) conjugated secondary antibody (Cat. # HAF007, R&D, UK) for one hour at 1 : 4000 (GAPDH), or goat anti-rabbit (Cat. # HAF008, R&D, UK) at 1 : 1000 (YAP). A molecular weight marker mPAGE® Color Protein Standard (Cat. # MPSTD4, Sigma-Aldrich, Switzerland) was used to identify the corresponding detected bands. Protein bands were visualised using the chemiluminescent HRP detection reagent Immobilon Forte Western HRP substrate (Cat. # WBLUF0020, Sigma-Aldrich, Switzerland). The optical density of the bands was estimated using ImageJ. The housekeeping protein GAPDH was used as a normalization control.

Statistical analysis

Particle size and zeta potential measurements are presented as mean ± standard deviation. Biological data including particle uptake, cell spreading and focal adhesion characteristics were collected from three biologically independent replicates and presented as mean + standard error of the mean. Statistical significance between conditions were determined using a one-way ANOVA with Tukey's *post hoc* test for multiple comparisons with a significance level of $p < 0.05$. Analysis was performed in Prism 9 (GraphPad Software).

Author contributions

A. L., D. S., P. T., C. L., B. R. and A. F. designed the study and wrote the manuscript. A. L. and D. M. performed particle synthesis and characterisation. A. L. prepared and characterised substrates. M. A. performed flow cytometry and western blot experiments. D. S., P. T. and C. L. provided scientific advice.

Conflicts of interest

The authors have no conflicts of interest to declare.

Acknowledgements

The authors are grateful to Dr Dimitri Vanhecke for discussions into cell visualization and labelling of adhesion processes. The authors would like to also thank Liliane Ackermann Hirschi, Laetitia Haeni and Shuiling Chu for their assistance with particle synthesis and cell culture. Microscopy and scattering analysis were performed on equipment provided by the Adolphe Merkle Institute, University of Fribourg, Switzerland. The authors would like to acknowledge the financial support of the NCCR Bioinspired Materials through the Swiss National Science Foundation and the Adolphe Merkle Foundation. D. S. acknowledges funding from SPARK through the Swiss National Science Foundation (190440).

References

1 P. H. Puech and P. Bongrand, Mechanotransduction as a major driver of cell behaviour: Mechanisms, and relevance to cell organization and future research, *Open Biol.*, 2021, **11**, 210256.
2 M. Selman and A. Pardo, Fibroageing: An ageing pathological feature driven by dysregulated extracellular matrix-cell mechanobiology, *Ageing Res. Rev.*, 2021, **70**, 101393.
3 Y. W. Zhou and Y. Wu, Substrate Viscoelasticity Amplifies Distinctions between Transient and Persistent LPS-Induced Signals, *Adv. Healthcare Mater.*, 2021, **11**, 2102271.
4 M. Amer, L. Shi and H. Wolfenson, The 'yin and yang' of cancer cell growth and mechanosensing, *Cancers*, 2021, **13**, 4754.
5 C. Yang, *et al.*, Spatially patterned matrix elasticity directs stem cell fate, *Proc. Natl. Acad. Sci. U. S. A.*, 2016, **113**, E4439–E4445.
6 A. Carnicer-Lombarte, *et al.*, Mechanical matching of implant to host minimises foreign body reaction. *bioRxiv*, 2019, 829648. DOI: **10.1101/829648**.
7 P. Foroozandeh and A. A. Aziz, Insight into Cellular Uptake and Intracellular Trafficking of Nanoparticles, *Nanoscale Res. Lett.*, 2018, **13**, 339.
8 A. C. Anselmo and S. Mitragotri, Impact of particle elasticity on particle-based drug delivery systems, *Adv. Drug Delivery Rev.*, 2017, **108**, 51–67.
9 Y. Hui, *et al.*, Role of Nanoparticle Mechanical Properties in Cancer Drug Delivery, *ACS Nano*, 2019, **13**, 7410–7424.
10 Z. Shen, H. Ye and Y. Li, Understanding receptor-mediated endocytosis of elastic nanoparticles through coarse grained molecular dynamic simulation, *Phys. Chem. Chem. Phys.*, 2018, **20**, 16372–16385.
11 J. Sun, *et al.*, Tunable rigidity of (polymeric core)-(lipid shell) nanoparticles for regulated cellular uptake, *Adv. Mater.*, 2015, **27**, 1402–1407.
12 A. Lee, *et al.*, Particle Stiffness and Surface Topography Determine Macrophage-Mediated Removal of Surface Adsorbed Particles, *Adv. Healthcare Mater.*, 2021, **10**, 2001667.
13 C. Huang, *et al.*, Substrate Stiffness Regulates Cellular Uptake of Nanoparticles, *Nano Lett.*, 2013, **13**, 1611–1615.
14 W. Xu, *et al.*, Cell Stiffness Is a Biomarker of the Metastatic Potential of Ovarian Cancer Cells, *PLoS One*, 2012, **7**, 46609.

15 S. Pal, Mechanical Properties of Biological Materials, in *Design of Artificial Human Joints & Organs*, Springer, Boston, MA, 2014, pp. 23–40. DOI: 10.1007/978-1-4614-6255-2_2.
16 P. Y. Wang, S. S. C. Hung, H. Thissen, P. Kingshott and R. C. B. Wong, Binary colloidal crystals (BCCs) as a feeder-free system to generate human induced pluripotent stem cells (hiPSCs), *Sci. Rep.*, 2016, **6**, 1–11.
17 T. Kyrey, *et al.*, Influence of the cross-linker content on adsorbed functionalised microgel coatings, *Polymer*, 2019, **169**, 29–35.
18 D. Septiadi, *et al.*, Particle Surfaces to Study Macrophage Adherence, Migration, and Clearance, *Adv. Funct. Mater.*, 2020, **30**, 2002630.
19 T. L. Moore, *et al.*, Nanoparticle administration method in cell culture alters particle-cell interaction, *Sci. Rep.*, 2019, **9**, 900.
20 M. J. Dalby, *et al.*, Attempted endocytosis of nano-environment produced by colloidal lithography by human fibroblasts, *Exp. Cell Res.*, 2004, **295**, 387–394.
21 W. Zhao, *et al.*, Nanoscale manipulation of membrane curvature for probing endocytosis in live cells, *Nat. Nanotechnol.*, 2017, **12**, 750–756.
22 H. Y. Lou, *et al.*, Membrane curvature underlies actin reorganization in response to nanoscale surface topography, *Proc. Natl. Acad. Sci. U. S. A.*, 2019, **116**, 23143–23151.
23 E. Susnik, *et al.*, Increased Uptake of Silica Nanoparticles in Inflamed Macrophages but Not upon Co-Exposure to Micron-Sized Particles, *Cells*, 2020, **9**, 9.
24 L. T. Zhuravlev, The surface chemistry of amorphous silica. Zhuravlev model, *Colloids Surf., A*, 2000, **173**, 1–38.
25 M. Sousa de Almeida, *et al.*, Cellular Uptake of Silica and Gold Nanoparticles Induces Early Activation of Nuclear Receptor NR4A1, *Nanomaterials*, 2022, **12**, 690.
26 L. Marichal, *et al.*, Protein Corona Composition of Silica Nanoparticles in Complex Media: Nanoparticle Size does not Matter, *Nanomaterials*, 2020, **10**, 240.
27 D. Zhao, *et al.*, Substrate stiffness regulated migration and angiogenesis potential of A549 cells and HUVECs, *J. Cell. Physiol.*, 2018, **233**, 3407–3417.
28 R. W. Tilghman, *et al.*, Matrix rigidity regulates cancer cell growth by modulating cellular metabolism and protein synthesis, *PLoS One*, 2012, **7**, e37231.
29 J. N. Lee, X. Jiang, D. Ryan and G. M. Whitesides, Compatibility of mammalian cells on surfaces of poly(dimethylsiloxane), *Langmuir*, 2004, **20**, 11684–11691.
30 D. Huh, *et al.*, Microfabrication of human organs-on-chips, *Nat. Protoc.*, 2013, **8**, 2135–2157.
31 A. Skardal, D. Mack, A. Atala and S. Sokern, Substrate elasticity controls cell proliferation, surface marker expression and motile phenotype in amniotic fluid-derived stem cells, *J. Mech. Behav. Biomed. Mater.*, 2013, **17**, 307–316.
32 B. Hinz, Mechanical Aspects of Lung Fibrosis A Spotlight on the Myofibroblast, *Proc. Am. Thorac. Soc.*, 2012, **9**(3), 137–147.
33 J. L. Leight, A. P. Drain and V. M. Weaver, Extracellular matrix remodeling and stiffening modulate tumor phenotype and treatment response, *Annu. Rev. Cancer Biol.*, 2017, **1**, 313–334.
34 L. Parisi, *et al.*, A glance on the role of fibronectin in controlling cell response at biomaterial interface, *Jpn. Dent. Sci. Rev.*, 2020, **56**, 50–55.
35 G. K. Toworfe, R. J. Composto, C. S. Adams, I. M. Shapiro and P. Ducheyne, Fibronectin adsorption on surface-activated poly(dimethylsiloxane) and its effect on cellular function, *J. Biomed. Mater. Res., Part A*, 2004, **71**, 449–461.
36 Y. Wang, T. Gong, Z.-R. R. Zhang and Y. Fu, Matrix Stiffness Differentially Regulates Cellular Uptake Behavior of Nanoparticles in Two Breast Cancer Cell Lines, *ACS Appl. Mater. Interfaces*, 2017, **9**, 25915–25928.
37 Q. Wei, *et al.*, Mechanotargeting: Mechanics-Dependent Cellular Uptake of Nanoparticles, *Adv. Mater.*, 2018, **30**, 1707464.
38 X. Wei, *et al.*, Mechanical cues modulate cellular uptake of nanoparticles in cancer via clathrin-mediated and caveolae-mediated endocytosis pathways, *Nanomedicine*, 2019, **8**, 613–626.
39 D. Septiadi, F. Crippa, T. L. Moore, B. Rothen-Rutishauser and A. Petri-Fink, Nanoparticle-Cell Interaction: A Cell Mechanics Perspective, *Adv. Mater.*, 2018, **30**, 1704463.
40 K. Iida, *et al.*, Cell softening in malignant progression of human lung cancer cells by activation of receptor tyrosine kinase AXL, *Sci. Rep.*, 2017, **7**, 1–11.
41 R. Sridharan, B. Cavanagh, A. R. Cameron, D. J. Kelly and F. J. O'Brien, Material stiffness influences the polarization state, function and migration mode of macrophages, *Acta Biomater.*, 2019, **89**, 47–59.
42 K. A. Jansen, P. Atherton and C. Ballestrem, Mechanotransduction at the cell-matrix interface, *Semin. Cell Dev. Biol.*, 2017, **71**, 75–83.
43 A. H. Williams, *et al.*, Bioscaffold Stiffness Mediates Aerosolized Nanoparticle Uptake in Lung Epithelial Cells, *ACS Appl. Mater. Interfaces*, 2021, **13**, 50643–50656.
44 L. E. Hind, M. Dembo and D. A. Hammer, Macrophage motility is driven by frontal-towing with a force magnitude dependent on substrate stiffness, *Integr. Biol.*, 2015, **7**, 447–453.
45 V. Malheiro, F. Lehner, V. Dinca, P. Hoffmann and K. Maniura-Weber, Convex and concave micro-structured silicone controls the shape, but not the polarization state of human macrophages, *Biomater. Sci.*, 2016, **4**, 1562–1573.
46 N. Jain, J. Moeller and V. Vogel, Mechanobiology of Macrophages: How Physical Factors Coregulate Macrophage Plasticity and Phagocytosis, *Annu. Rev. Biomed. Eng.*, 2019, **21**, 267–297.
47 T. Wiegand, *et al.*, Forces during cellular uptake of viruses and nanoparticles at the ventral side, *Nat. Commun.*, 2020, **11**, 1–13.
48 D. J. Leahy, I. Aukhil and H. P. Erickson, 2.0 Å crystal structure of a four-domain segment of human fibronectin encompassing the RGD loop and synergy region, *Cell*, 1996, **84**, 155–164.

49 T. Petithory, *et al.*, Size-dependent internalization efficiency of macrophages from adsorbed nanoparticle-based monolayers, *Nanomaterials*, 2021, **11**, 1963.
50 R. Hartmann, M. Weidenbach, M. Neubauer, A. Fery and W. J. Parak, Stiffness-dependent in vitro uptake and lysosomal acidification of colloidal particles, *Angew. Chem., Int. Ed.*, 2015, **54**, 1365–1368.
51 U. Horzum, B. Ozdil and D. Pesen-Okvur, Step-by-step quantitative analysis of focal adhesions, *MethodsX*, 2014, **1**, 56–59.
52 I.-L. Hsiao, *et al.*, Size and cell type dependent uptake of silica nanoparticles, *J. Nanomed. Nanotechnol.*, 2014, **5**, 1000248.
53 J. Song, *et al.*, Role of YAP in lung cancer resistance to cisplatin, *Oncol. Lett.*, 2018, **16**, 3949–3954.
54 V. Rausch and C. G. Hansen, The Hippo Pathway, YAP/TAZ, and the Plasma Membrane, *Trends Cell Biol.*, 2020, **30**, 32–48.
55 J. R. Davis and N. Tapon, Hippo signalling during development, *Development*, 2019, **146**, dev167106.
56 R. Strippoli, *et al.*, Caveolin1 and YAP drive mechanically induced mesothelial to mesenchymal transition and fibrosis, *Cell Death Dis.*, 2020, **11**, 1–19.
57 V. Rausch, *et al.*, The Hippo Pathway Regulates Caveolae Expression and Mediates Flow Response via Caveolae, *Curr. Biol.*, 2019, **29**, 242–255.
58 B. King, J. Araki, W. Palm and C. B. Thompson, Yap/Taz promote the scavenging of extracellular nutrients through macropinocytosis, *Genes Dev.*, 2020, **34**, 1345–1358.
59 Y. C. Yeh, J. Y. Ling, W. C. Chen, H. H. Lin and M. J. Tang, Mechanotransduction of matrix stiffness in regulation of focal adhesion size and number: Reciprocal regulation of caveolin-1 and β1 integrin, *Sci. Rep.*, 2017, **7**, 1–14.
60 X. Li, *et al.*, Nanoscale Surface Topography Reduces Focal Adhesions and Cell Stiffness by Enhancing Integrin Endocytosis, *Nano Lett.*, 2021, **21**, 8518–8526.
61 G. Nardone, *et al.*, YAP regulates cell mechanics by controlling focal adhesion assembly, *Nat. Commun.*, 2017, **8**, 1–13.
62 D. E. Mason, *et al.*, YAP and TAZ limit cytoskeletal and focal adhesion maturation to enable persistent cell motility, *J. Cell Biol.*, 2019, **218**, 1369–1389.
63 X. Tan, J. Heureaux and A. P. Liu, Cell spreading area regulates clathrin-coated pit dynamics on micropatterned substrate, *Integr. Biol.*, 2015, **7**, 1033.
64 M. Sousa De Almeida, *et al.*, Understanding nanoparticle endocytosis to improve targeting strategies in nanomedicine, *Chem. Soc. Rev.*, 2021, **50**, 5397–5434.
65 R. Moreno-Vincente, *et al.*, Caveolin-1 Modulates Mechanotransduction Responses to Substrate Stiffness through Actin-Dependent Control of YAP, *Cell Rep.*, 2018, **25**, 1622–1635.
66 Y. Wang, *et al.*, Overexpression of yes-associated protein contributes to progression and poor prognosis of non-small-cell lung cancer, *Cancer Sci.*, 2010, **101**, 1279–1285.
67 M. Yu, *et al.*, YAP1 contributes to NSCLC invasion and migration by promoting Slug transcription via the transcription co-factor TEAD, *Cell Death Dis.*, 2018, **9**, 464.
68 M. Shreberk-Shaked, *et al.*, A Division of Labor between YAP and TAZ in Non-Small Cell Lung Cancer, *Cancer Res.*, 2020, **80**, 4145–4157.
69 F. Baschieri, *et al.*, Frustrated endocytosis controls contractility-independent mechanotransduction at clathrin-coated structures, *Nat. Commun.*, 2018, **9**, 1–13.
70 J. G. Joseph and A. P. Liu, Mechanical Regulation of Endocytosis: New Insights and Recent Advances, *Adv. Biosyst.*, 2020, **4**, e1900278.
71 W. Stober and A. Fink, Controlled Growth of Monodispersed Silica Spheres in the Micron Size Range, *J. Colloid Interface Sci.*, 1968, **26**, 62–69.
72 K. Mohr, *et al.*, Evaluation of multifunctional liposomes in human blood serum by light scattering, *Langmuir*, 2014, **30**, 14954–14962.
73 A. B. C. Buskermolen, N. A. Kurniawan and C. V. C. Bouten, An automated quantitative analysis of cell, nucleus and focal adhesion morphology, *PLoS One*, 2018, **13**, e0195201.